Quality Assessment of the Experimental Data of Wood Structure Using Kanpur Theorem

Anand Shukla, Manabendra Saha, and Richa Dixit

1 Introduction

Computerized tomography (CT) has turned out to be a standard method for examination in the fields of material sciences and medicine. The principal advantage of CT imaging over conventional technique is that it permits detection and quantification of heterogeneities and internal defects for material density determination.

As CBP algorithm is the foundation of CT scanners used in NDE for computerized tomography, convolution backprojection (CBP), a reconstruction algorithm, is used to reconstruct the object cross section. This algorithm makes use of filter functions, which are user-dependent. For the same dataset, different filter functions lead to different reconstruction. This is followed from the mathematical formulation of the CBP algorithm, and it can be demonstrated that for a reconstruction process, the reconstruction with any given filter will lead to a theoretical error. In the initials days of CT imaging, Natterer [1] gave an account of a mathematical study, which showed the probable use of Sobolev-space techniques for inferring the errors involved in the tomographic reconstruction process, which resulted the final CT images from the gamma-ray (X-ray) projection data. Munshi et al. [2, 3] carried out the further work on error theorems.

First Kanpur theorem gives the user with a quantitative estimate of the local error in the CT image, and second Kanpur theorem informs about global error obtained by most engineering/medical scanners. Second level of reconstructions (acquired by original CT images) gives an error estimate that is not achievable otherwise. This approach results in very useful tools for quantification of nature of internal defects in the engineering materials as well as in human tissues.

A. Shukla (✉) · M. Saha
ABES Engineering College, Dr. A.P.J. Abdul Kalam Technical University, Ghaziabad, India
e-mail: anand.srcem@gmail.com

R. Dixit
St. Aloysius College, Rani Durgawati University, Jabalpur, India

K. Kumar Singh et al. (eds.), *Machine Vision and Augmented Intelligence*, Lecture Notes in Electrical Engineering 1007, https://doi.org/10.1007/978-981-99-0189-0_17

1.1 Theoretical Background of CT

The ray travels from source to detector through object in X-ray tomography. When these rays passes through a part of an object, it gets the information of it. To scan whole object, the source and detector are rotated around it for large number of views. From these projection data stored in detector, distribution of few properties like attenuation coefficients within the object is reconstructed making use of the reconstruction techniques.

The objective of CT is to get information regarding the nature of the material occupying exact positions inside the component or body. To obtain information, every point inside the body is allotted a number which is particular to the material occupying that part. A fit candidate for this number is the material's X-ray attenuation coefficient (Fig. 1).

The relation between intensities I_{in} and I_{out} shown in Fig. 1 is given according to *Lambert–Beer* law as

$$I_{out} = I_{in} \exp\left(-\int_L f(x, y)\mathrm{d}l\right) \tag{1}$$

Application of natural log both sides gives

$$\ln\left[\frac{I_{in}}{I_{out}}\right] = \int (f(x, y))\mathrm{d}l \tag{2}$$

This implies that the detector detects line integral of the object function along a particular line and for a specific view. To get the full extent of the whole object function, the line integral is collected for many numbers of rays at different angles. In case of X-ray CT, the attenuation coefficient, $\mu(x, y)$, which is the characteristics of the object is represented by the object function, $f(x, y)$.

The attenuation of X-ray beam primarily occur either because of scattering from their original direction of travel or due to absorption by the atoms of material. The accountable mechanisms for this attenuation are Compton effect and photoelectric effect, respectively. Munshi [2] has made an effort to estimate errors occurring

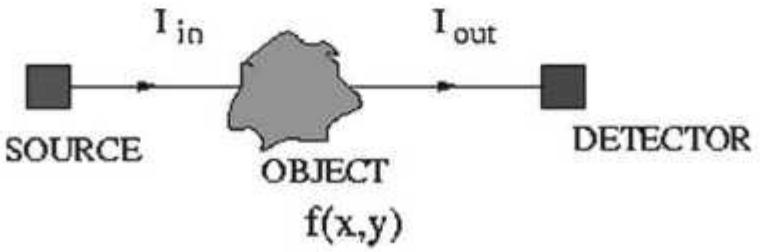

Fig. 1 X-ray attenuation through the object

in different tomographic algorithms under the supposition that the object cross-section posses band-limited projection data. In the study, he evolved a simplified two-dimensional Cartesian formula (KT-1) for predicting the comparative performance of the Fourier filters used in the convolution back projection algorithm. This approach involves the Laplacian of the object function and the second-order derivatives of the filter functions. The norms are local in character rather than the global norms in this study.

Herman [4] has categorized and explored the computational and mathematical procedures underlying the data collection, image reconstruction, and image display in practice of computerized tomography. He also described the reconstruction algorithms and presented the treatment of the computational problems linked with the display of the results. The methods for estimation of error incurred in reconstruction method are explained in details too.

Radon [5] has given a radon inversion formula derived in 1971 which helped to solve the problem of image reconstruction from the projection data. In an experiment, the datasets gathered by detectors are the set of line integrals along a particular line passing through the object cross section. Radon also proved that any arbitrary function could be retrieved from its set of line integrals taken along various chords and various directions.

All the studies mentioned above make use of the methods to estimate the inherent error incurred in the reconstruction of images. The theorems by Munshi et al. [6, 7] are known as Kanpur Error Theorem that gives the formula to estimate the inherent error. The present study aims at detection and quantification of internal disease of the body parts by applying Kanpur Error Theorems on scanned images.

2 Material and Methods

Projection data is required for the reconstruction of object function $\mu(x, y)$. There are two modes mainly used for projection data collection, called parallel beam geometry (PBG) and fan beam geometry (FBG).

(a) Parallel beam geometry

PBG mode of data collection comprises several pairs of radiation source and detector system, using which the object can be scanned completely. The object to be scanned is placed on a table, which can be rotated for giving different views, and the source-detector pairs are spaced uniformly. The SD (source detector) line represents the data ray path. The angle of the source position (or object rotation) is denoted by θ and the perpendicular distance of the ray from the origin is denoted by 's'. PBG setup is represented in Fig. 2.

(b) Fan beam geometry

All medical and industrial scanners incorporate the FBG mode collection mechanism, which involves a rotating module including a source and array of detectors placed in

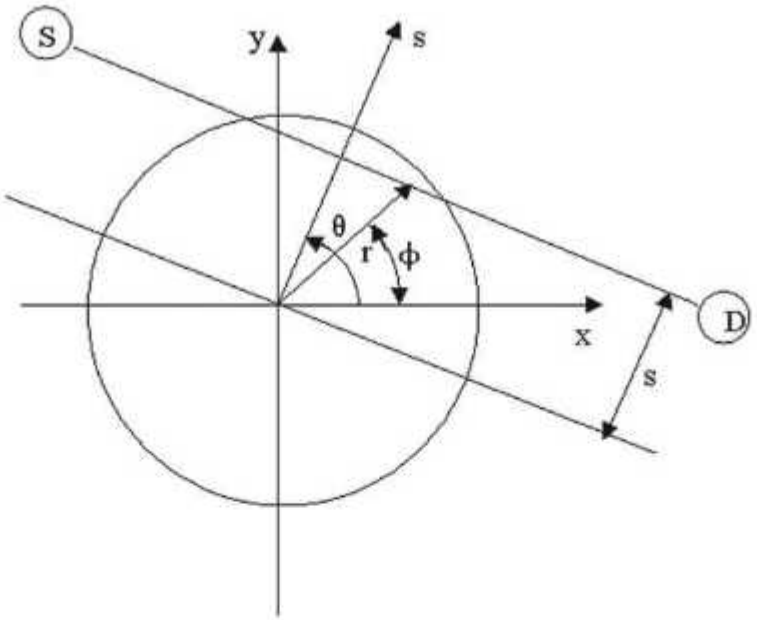

Fig. 2 Parallel beam geometry

an arc around the object. FBG configuration is shown in Fig. 3. For computational feasibility of reconstruction algorithms, the projection data collected in FBG, i.e., $g(\rho, \beta)$, must be converted into PBG '$p(s, \theta)$.

Projection data collected from the detectors '$p(s, \theta)$, of an object $f(x, y)$, is actually the radon transform $R\ f(s.\theta)$, and is equivalent to line integrals through the object in all possible directions. That is, a single radon value is the integral of all points along a line with angle θ and perpendicular distance 's' from the origin, as shown in Fig. 4.

The radon transform can be written as:

$$p(s, \theta) = R\, f(s, \theta) = \int \int f(x, y)\, \delta\,(x \cos\theta + y \sin\theta - s)\mathrm{d}x\, \mathrm{d}y \qquad (3)$$

The correlation between the Fourier transform and the radon transform is given by the Fourier slice theorem. This theorem states "one dimensional Fourier transform of the Radon transform along a radial line is identical to the same line in the two dimensional Fourier transforms of the object." The theorem, illustrated in Fig. 5, mathematically, is written as:

$$F_1 R\, f(R, \theta) = F_2 R\, f(R\cos\theta,\ R\sin\theta) \qquad (4)$$

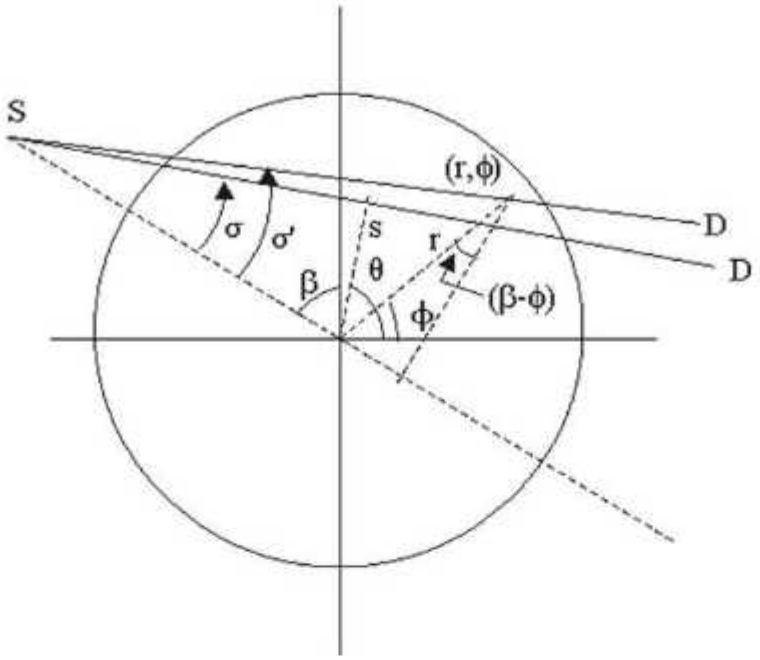

Fig. 3 Fan beam geometry

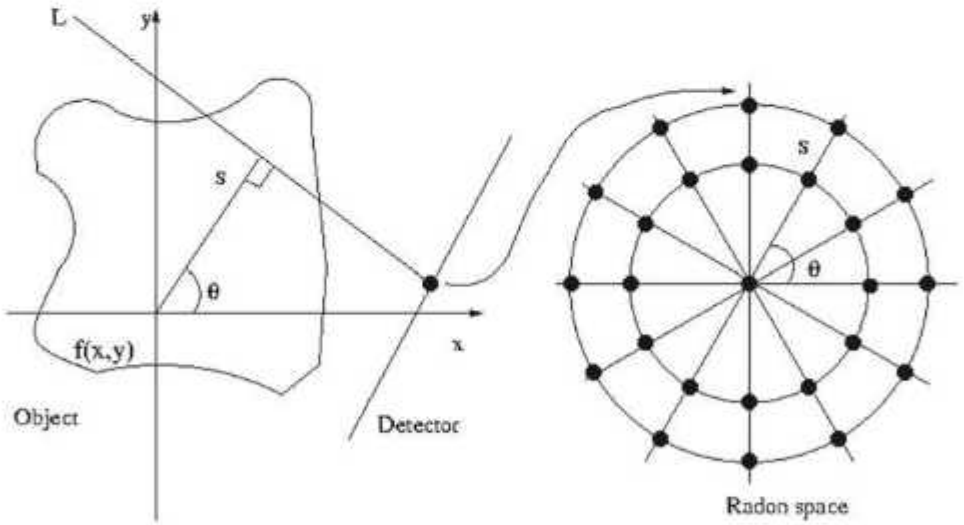

Fig. 4 Radon value is the line integral along the line *L*

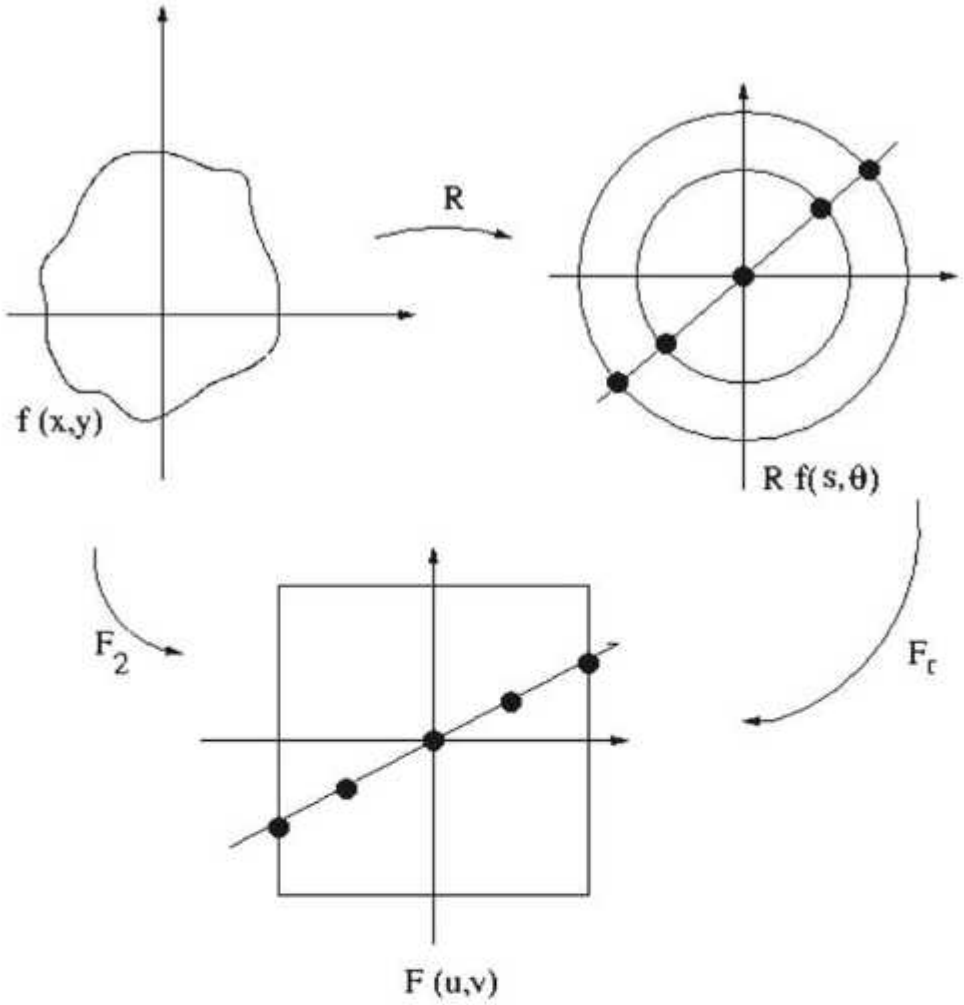

Fig. 5 The Fourier slice theorem

2.1 Image Reconstruction from Projections

The application range of image reconstruction is very wide. Shown in Fig. 6 is the computation of the inverse radon transform. Object function is evaluated using inverse radon transform from the given projection data.

Image reconstruction is very appropriately defined in words of Herman [4] as: "Image reconstruction from projections is the process of producing an image of a two dimensional distribution (usually of some physical property) from estimates of its line integrals along a finite number of lines of known locations".

CT numbers from the projection data is obtained using this method. A mathematical formula for image reconstruction was given by radon. For its evaluation, an efficient algorithm is needed. There has been a lot of activity in the past years to

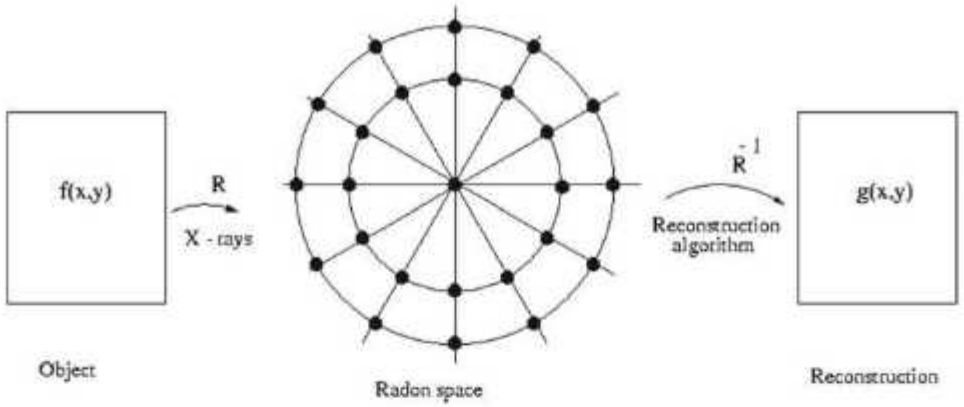

Fig. 6 Computing inverse of the Radon transform

find algorithms that are fast when implemented on a computer and which produce acceptable reconstructions despite the finite and inaccurate nature of the projection data. Reconstruction algorithms are chiefly categorized into two basic groups:

(a) Transform methods and
(b) Series expansion methods.

Convolution back projection (CBP) is one such algorithm coming under former category and is used most of the times for medical and NDT applications. Filtering of projection data is incorporated in CBP. There are many filter functions and the choice of which is dependent on user. Different filter functions result in different reconstructions for the same set of projection data.

3 Results and Discussions

3.1 First Kanpur Error Theorem (KT-1)

The projection data is not band-limited because the objects being reconstructed usually have a finite support. However, the reconstruction approximation obtained is band-limited due to a finite Fourier cut-off frequency, incorporated for computational feasibility. Hence, the inherent error arises from this band-limiting aspect. This error can be predicted with the help of First Kanpur theorem. It is local by nature and is an excellent tool for quantification of reconstruction. It shows point-wise error. Shown in Maisl et al. [8] is that if $N_{\max}$ represents the maximum value of grey level in reconstruction then the overall error is directly proportional to $1/N_{\max}$. In the simplified form, this theorem says that the overall error ($1/N_{\max}$) in reconstruction is directly proportional to the second order partial derivative of filter function at Fourier space origin $W''(0)$, The KT-I theorem is local in nature, hence, deals with every pixel to

pixel error. *This theorem provides a very good idea of overall error incurred even if original cross section is not known, which is also the case in all real-life situations.*

Two samples of Palash and Rosewood of 1 cm × 1 cm × 1 cm are scanned using CT-Mini micro-CT scanner. Further, two slices both of Palash and Rosewood are selected randomly for validation of experiment. For each slice, the image reconstruction is done with the help of five filters, namely, Hann, Hamming, Cosine, Shepp-Logan, and Ram-Lac.

3.2 Palash

(1) Slice 692

Figure 7a–f shows original and reconstructed images using Hann, Hamming, Cosine, Shepp-Logan, and Ram-Lac filters, respectively. Others parameters used are same for all reconstructed images, e.g., dimensions of mesh, interpolation, span, etc. It can be seen that, for Palash, a bigger central hole is present and fibers are distributed about it unsymmetrically. Further, it can be observed that gray level of reconstructed images changes with different filters.

Table 1 shows $N_{\max}$, i.e., maximum value of gray level for the reconstructed images using different filters. For Hann, it is 260.9750, for Hamming it is 263.2942, for Cosine it is 276.2953, for Shepp-Logan it is 285.4775, and Ram-Lac it is 292.9257.

Table 2 gives values of $W''(0)$ for different filters used in image reconstruction. The window function $W(\alpha)$ is related to filter parameter α as

$$W(\alpha) = \alpha + (1 - \alpha) \sin c(\alpha/1 - \alpha) \tag{1}$$

Hence, $W''(0)$ can be found for each filter used.

Figure 8 shows the KT plot of $1/N_{\max}$ versus $W''(0)$. The x axis represents $W''(0)$ and y axis represents $1/N_{\max}$. The plotted points are very close to fitted straight line. Table 3 provides the slope and intercept of the fitted straight line which are equal to 0.00082 and 0.0034, respectively. The resultant "Goodness of Fit" comes out to be 99.18.

For Palash slice 692, slope = 0.00082.

Hence, its Goodness of Fit = 100 * (1 − 0.00082) = 99.18.

(2) Slice 912

Figure 9a–f shows original and reconstructed images using Hann, Hamming, Cosine, Shepp-Logan, and Ram-Lac filters, respectively. Others parameters used are same for all reconstructed images, e.g., dimensions of mesh, interpolation, span, etc. Again for this slice of Palash also, it can be seen that a bigger central hole is present and fibers are distributed about it unsymmetrically. Further, it can be observed that gray level of reconstructed images changes with different filters.

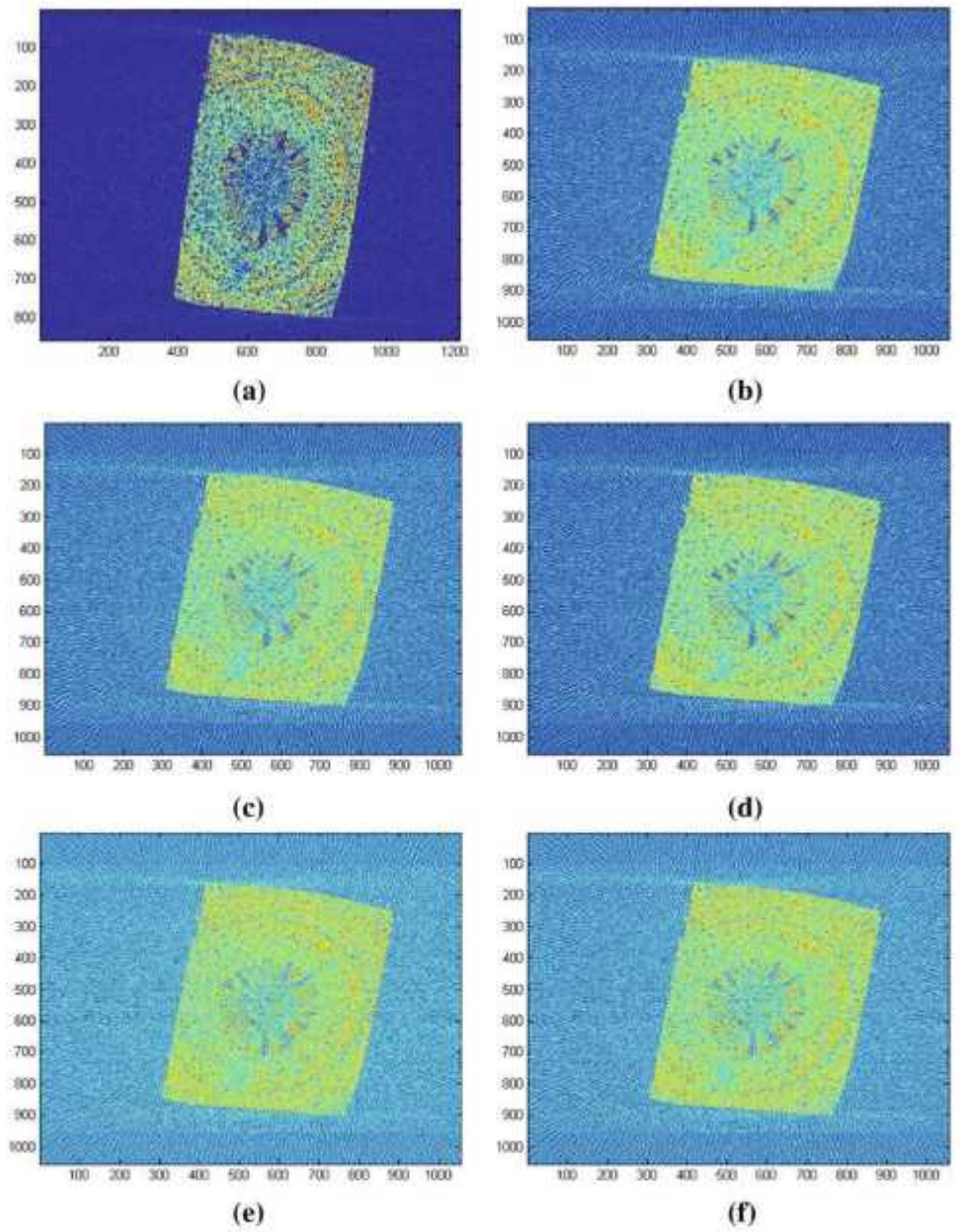

Fig. 7 Original and reconstructed images of Palash slice 692 **a** Original **b** Hann **c** Hamming **d** Cosine **e** Shepp-Logan **f** Ram-Lak

Table 4 shows N_{max}, i.e., maximum value of gray level for the reconstructed images using different filters. For Hann, it is 268.2430, for Hamming it is 270.3833, for Cosine it is 282.5012, for Shepp-Logan it is 298.7857, and Ram-Lac it is 310.1384. Table 5 gives values of $W''(0)$ for different filters used in image reconstruction. It remains same as that of Table 2.

Table 1 $1/N_{max}$ values for reconstructed images using different filters

S. No.	Filter used	N_{max}	$1/N_{max}$
1	Hann	260.9750	0.0038
2	Hamming	263.2942	0.0038
3	Cosine	276.2953	0.0036
4	Shepp-Logan	285.4775	0.0035
5	Ram-Lak	292.9257	0.0034

Table 2 Values of $W''(0)$ for different filters

S. No.	Filter used	α	$W''(0)$
1	Hann	0.50	0.50
2	Hamming	0.54	0.46
3	Cosine	0.75	0.25
4	Shepp-Logan	0.91	0.09
5	Ram-Lak	0.99	0.01

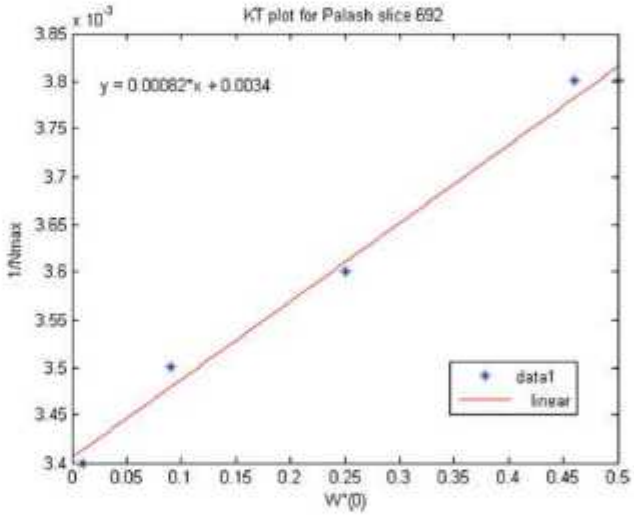

Fig. 8 KT plot for Palash slice 692

Table 3 Slope and intercept of the KT1 plot for Palash slice 692

S. No.	Slope	Intercept
1	0.00082	0.0034

Figure 10 shows the KT plot of $1/N_{max}$ versus $W''(0)$. The x axis represents $W''(0)$, and y axis represents $1/N_{max}$. The plotted points are very close to fitted straight line. Table 6 provides the slope and intercept of the fitted straight line which are equal to 0.001 and 0.0032, respectively. The resultant "Goodness of Fit" comes out to be 99.9.

For Palash slice 912, slope = 0.001.

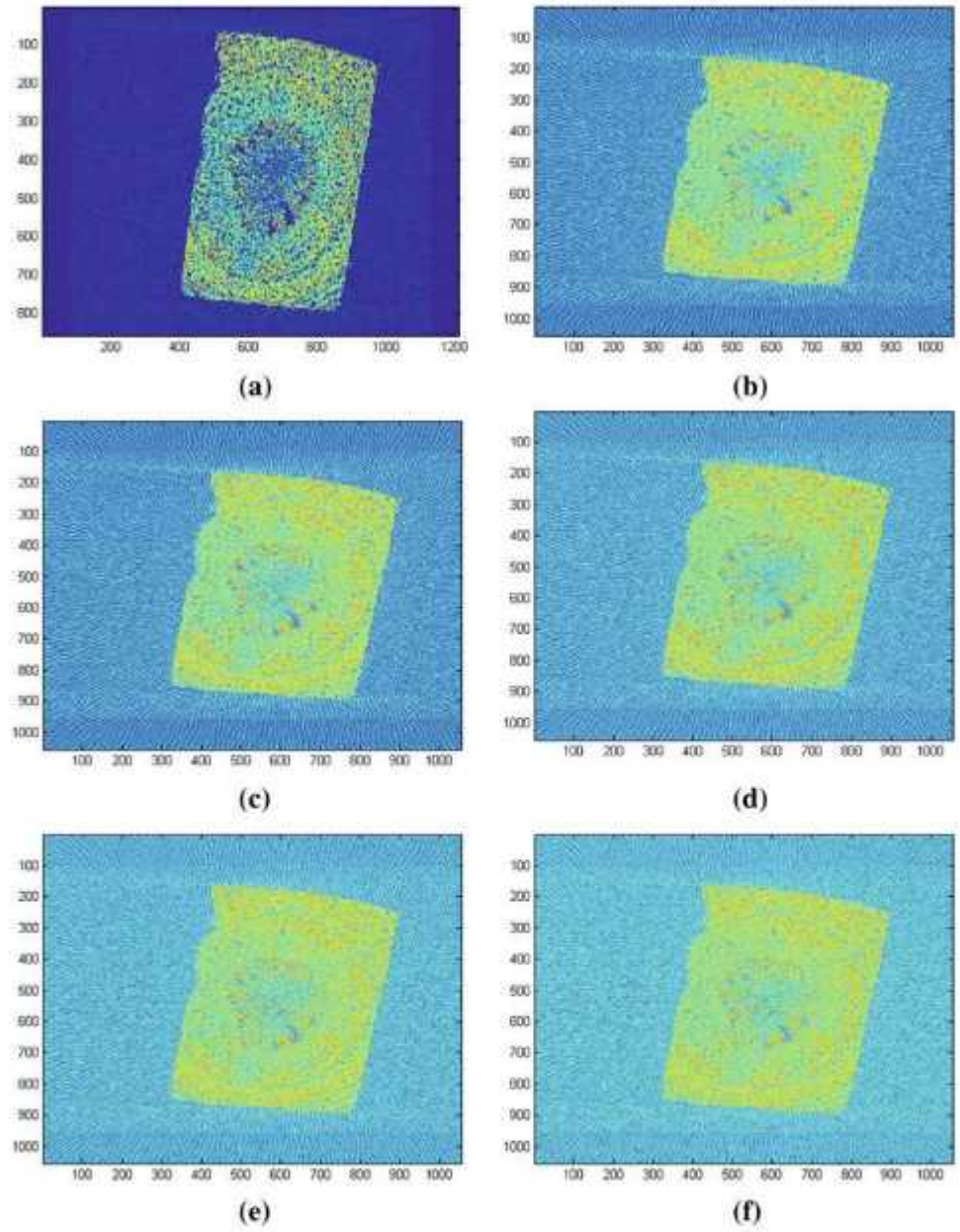

Fig. 9 Original and reconstructed images of Palash slice 912 **a** Original **b** Hann **c** Hamming **d** Cosine **e** Shepp-Logan **f** Ram-Lak

Hence, its Goodness of Fit = 100*(1 − 0.001) = 99.9.

Table 4 $1/N_{max}$ values for reconstructed images using different filters

S. No.	Filter used	N_{max}	$1/N_{max}$
1	Hann	268.2430	0.0037
2	Hamming	270.3833	0.0037
3	Cosine	282.5012	0.0035
4	Shepp-Logan	298.7857	0.0033
5	Ram-Lak	310.1384	0.0032

Table 5 Values of $W''(0)$ for different filters

S. No.	Filter used	α	$W''(0)$
1	Hann	0.50	0.50
2	Hamming	0.54	0.46
3	Cosine	0.75	0.25
4	Shepp-Logan	0.91	0.09
5	Ram-Lak	0.99	0.01

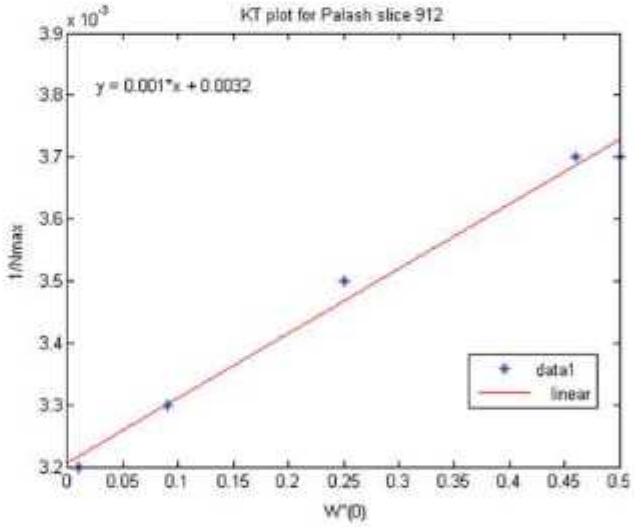

Fig. 10 KT plot for Palash slice 912

Table 6 Slope and intercept of the KT1 plot for Palash slice 912

S. No.	Slope	Intercept
1	0.001	0.0032

3.3 Rosewood

(1) **Slice 448**

Figure 11a–f shows original and reconstructed images using Hann, Hamming, Cosine, Shepp-Logan, and Ram-Lac filters, respectively. Others parameters used

are same for all reconstructed images, e.g., dimensions of mesh, interpolation, span, etc. For Rosewood, it can be seen that a small central hole is present and fibers are distributed about it symmetrically. Further, it can be observed that gray level of reconstructed images changes with different filters.

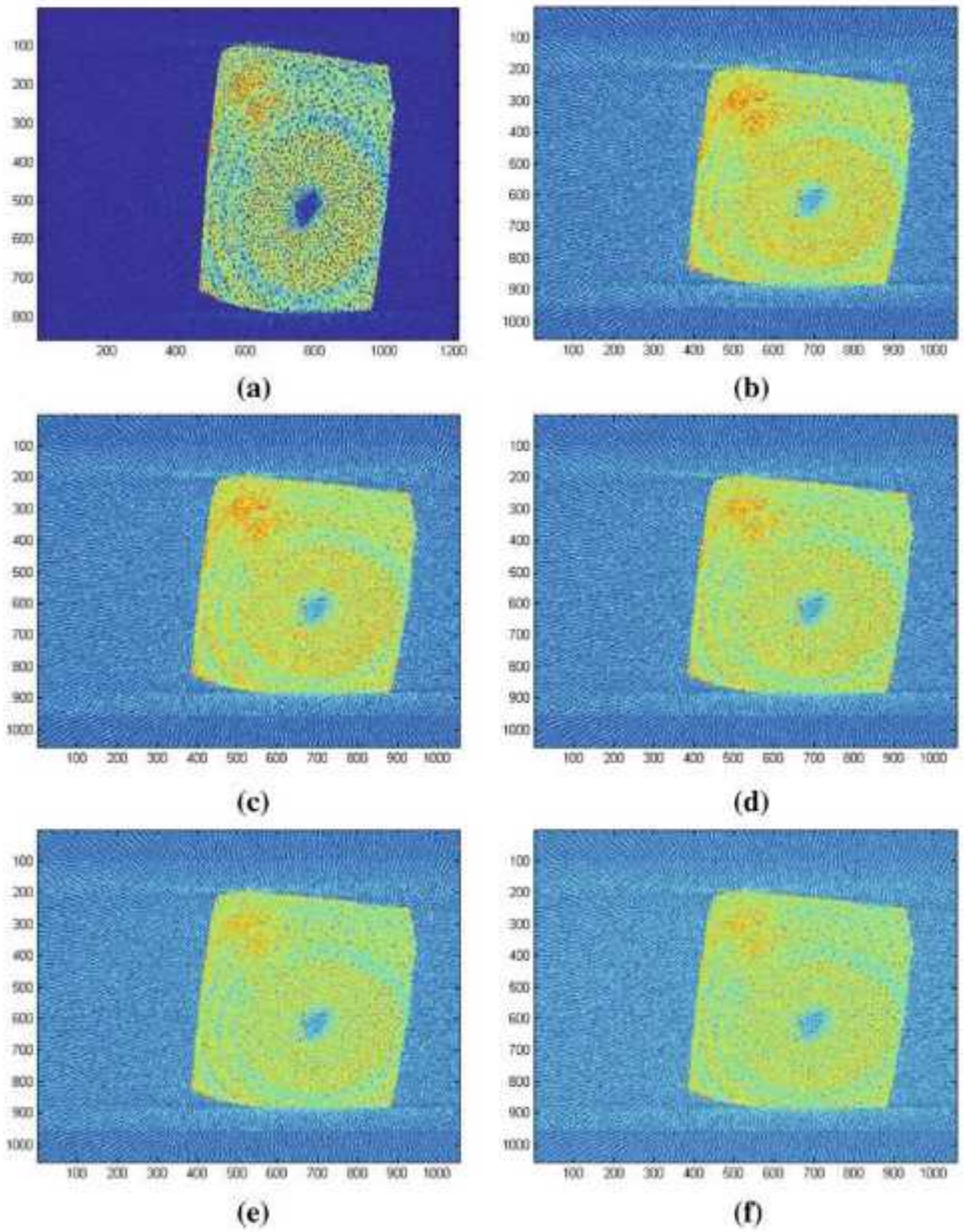

Fig. 11 Original and reconstructed images of Rosewood slice 448 **a** Original **b** Hann **c** Hamming **d** Cosine **e** Shepp-Logan **f** Ram-Lak

Table 7 $1/N_{max}$ values for reconstructed images using different filters

S. No.	Filter used	N_{max}	$1/N_{max}$
1	Hann	206.4679	0.0048
2	Hamming	209.9287	0.0048
3	Cosine	223.1424	0.0045
4	Shepp-Logan	240.6033	0.0042
5	Ram-Lak	249.7281	0.0040

Table 8 Values of $W''(0)$ for different filters

S. No.	Filter used	α	$W''(0)$
1	Hann	0.50	0.50
2	Hamming	0.54	0.46
3	Cosine	0.75	0.25
4	Shepp-Logan	0.91	0.09
5	Ram-Lak	0.99	0.01

Table 7 shows N_{max}, i.e., maximum value of gray level for the reconstructed images using different filters. For Hann, it is 268.2430, for Hamming it is 270.3833, for Cosine it is 282.5012, for Shepp-Logan it is 298.7857 and Ram-Lac it is 310.1384. Table 8 gives values of $W''(0)$ for different filters used in image reconstruction. It remains same as that of Table 2.

Figure 12 shows the KT plot of $1/N_{max}$ versus $W''(0)$. The x axis represents $W''(0)$, and y axis represents $1/N_{max}$. The plotted points are very close to fitted straight line. Table 9 provides the slope and intercept of the fitted straight line which are equal to 0.001 and 0.0032, respectively. The resultant "Goodness of Fit" comes out to be 99.9.

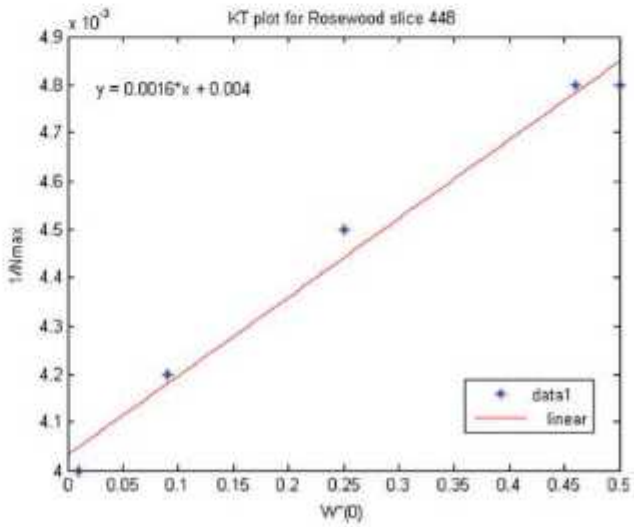

Fig. 12 KT plot for Rosewood slice 448

Table 9 Slope and intercept of the KT1 plot for Rosewood slice 448

S. No.	Slope	Intercept
1	0.0016	0.004

For Rosewood slice 448, slope = 0.0016.
Hence, its Goodness of Fit = 100 * (1 − 0.0016) = 99.84.

(2) **Slice 591**

Figure 13a–f shows original and reconstructed images using Hann, Hamming, Cosine, Shepp-Logan, and Ram-Lac filters, respectively. Others parameters used are same for all reconstructed images, e.g., dimensions of mesh, interpolation, span, etc. Again, for this Rosewood also, it can be seen that a small central hole is present and fibers are distributed about it symmetrically. Further, it can be observed that gray level of reconstructed images changes with different filters.

Table 10 shows N_{max}, i.e., maximum value of gray level for the reconstructed images using different filters. For Hann, it is 207.4564, for Hamming it is 209.7615, for Cosine it is 222.0279, for Shepp-Logan it is 231.5470, and Ram-Lac it is 236.3579. Table 11 gives values of $W''(0)$ for different filters used in image reconstruction. It remains same as that of Table 2.

Figure 14 shows the KT plot of $1/N_{max}$ versus $W''(0)$. The x axis represents $W''(0)$, and y axis represents $1/N_{max}$. The plotted points are very close to fitted straight line. Table 12 provides the slope and intercept of the fitted straight line which are equal to 0.0013 and 0.0042, respectively. The resultant "Goodness of Fit" comes out to be 99.87.

For Rosewood slice 591, slope = 0.0013.
Hence, its Goodness of Fit = 100 * (1 − 0.0013) = 99.87.

4 Conclusion

A scanning experiment is performed on samples of Palash and Rosewood of 1 cm × 1 cm × 1 cm each using CT-Mini micro-CT scanner, and a corresponding dataset is obtained. The dataset, also called the projection data, comprises 180 scans corresponding to 180° rotation of the object (i.e., 1 scan per degree of rotation) within the 'Field of View' of Source-detector system. It is actually $\ln[I_{in}/I_{out}]$, which theoretically should be equal to radon transform of object function 'f', i.e., $\int f(x, y)dl$.

This dataset is used in a program of image reconstruction, and an image is reconstructed. We call this as 'original-image'. This 'original image' has been used as the object itself. *Kanpur theorem*-1 could not be applied on experimental dataset itself, and $1/N_{max}$ versus $W''(0)$ could not be plotted because it was not known if the dataset is the outcome of an experiment complying a scientific law (here *Lambert–Beer* law) or not. It might have been corrupted by an experimental error, or some

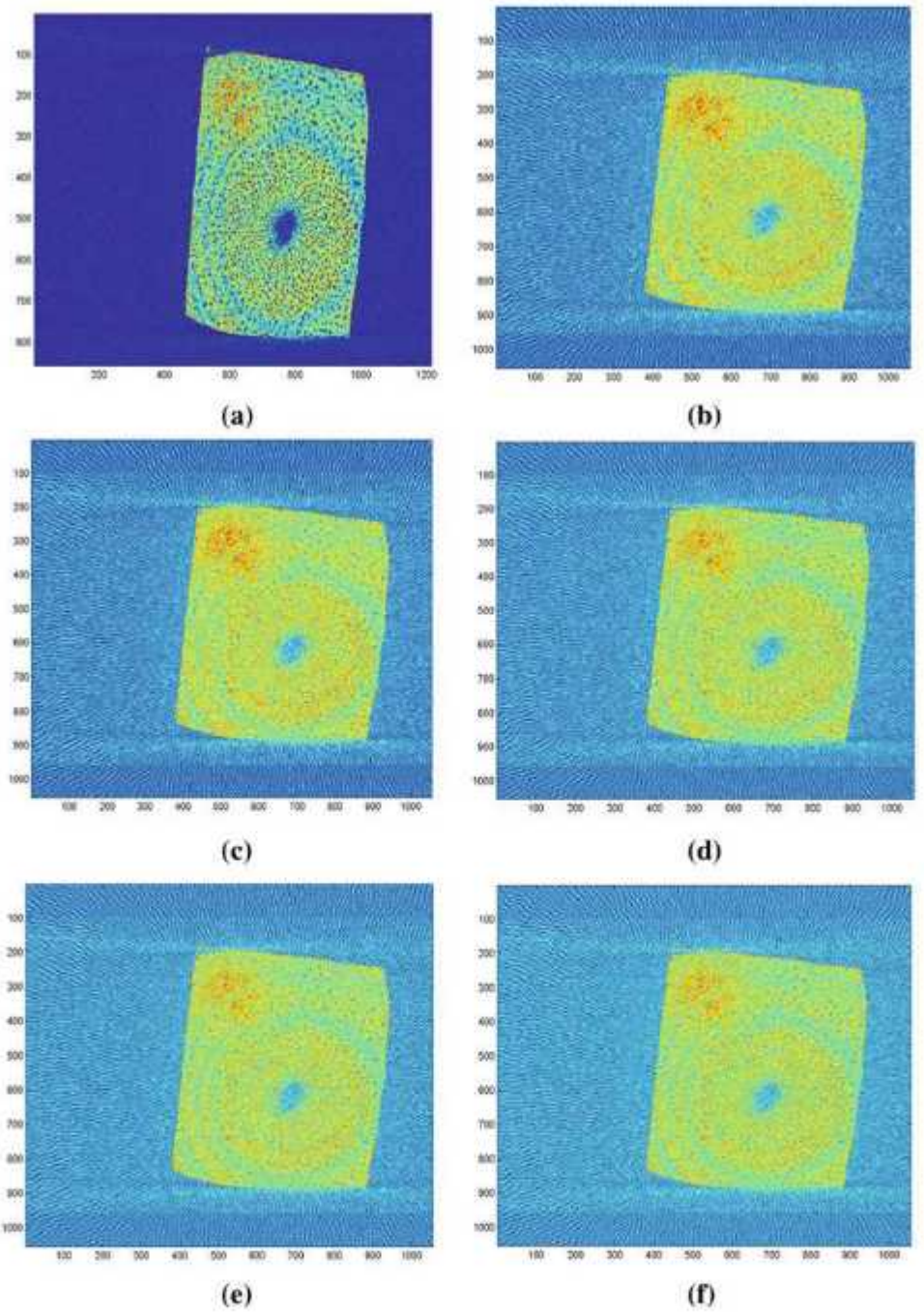

Fig. 13 Original and reconstructed images of Rosewood slice 591 **a** Original **b** Hann **c** Hamming **d** Cosine **e** Shepp-Logan **f** Ram-Lak

Table 10 $1/N_{max}$ values for reconstructed images using different filters

S. No.	Filter used	N_{max}	$1/N_{max}$
1	Hann	207.4564	0.0048
2	Hamming	209.7615	0.0048
3	Cosine	222.0279	0.0045
4	Shepp-Logan	231.5470	0.0043
5	Ram-Lak	236.3579	0.0042

Table 11 Values of $W''(0)$ for different filters

S. No.	Filter used	α	$W''(0)$
1	Hann	0.50	0.50
2	Hamming	0.54	0.46
3	Cosine	0.75	0.25
4	Shepp-Logan	0.91	0.09
5	Ram-Lak	0.99	0.01

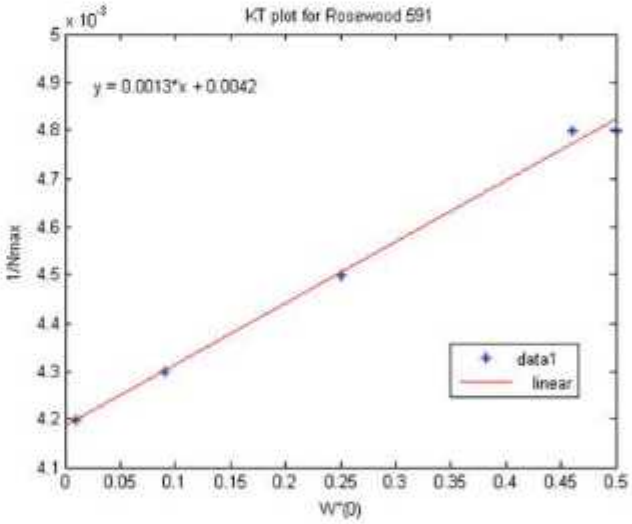

Fig. 14 KT plot for Rosewood slice 591

Table 12 Slope and intercept of the KT1 plot for Rosewood slice 591

S. No.	Slope	Intercept
1	0.0013	0.0042

intentional/unintentional modification had affected it. The scanner had just given $\ln[I_{in}/I_{out}]$, which we could not assume to be equal to $\int f(x, y)dl$ without validating the experiment.

On considering the 'original image' as an object itself, hardly an error of 3% could be introduced. Hence, it could be safely considered to be an object with a small inherent error. Now, using MATLAB, the radon transform of this original

image, i.e., $\int f(x, y)dl$ is done, and hence a new dataset gets generated. If there is no experimental error, then this new dataset would be approximately equal to the dataset obtained via experiment.

Now, the Fourier transform of the new dataset is taken, five filters are applied one by one, and two-dimensional inverse Fourier transform is taken to generate five reconstructed images finally. For each image, $N_{\max}$ is calculated, and a plot of $1/N_{\max}$ (which is proportional to error) versus second derivative of filter function at origin, i.e., $W''(0)$ is drawn with the help of MATLAB. If the reconstructed image only has inherent errors (propagated by considering original image as an object and arising due to use of filters), then the plots should have points very close to the fitted line and occurring at fixed spacing from it. But if there are experimental errors, then the filters can behave arbitrarily on their edges, and the plots will have points that are randomly spaced from the line. Hence, with this process, one can judge the quality of image and conclude if the experiment performed is free of errors or not. It should also be noted that in entire process, we are assuming discretization error to be almost negligible.

The most important benefit of this work is that it provides a precise method of predicting the quality of reconstructed image in computerized tomography, and hence one can determine if the experiment is required to be performed again or not. Further on an application note, this method can facilitate comparison of inner structure of two objects very easily and accurately.

References

1. Natterer F (1986) The mathematics of computerized tomography. Wiley, New York
2. Munshi P (1992) Error analysis of tomographic filters I: theory. NDT&E Int 25(4/5):191
3. Munshi P, Rathore RKS, Ram KS, Kalra MS (1991) Error estimates for Tomographic inversion. Inverse Prob 7:399
4. Herman GT (1980) Image reconstruction from projections: the fundamentals of computerized tomography. Academic, New York
5. Radon J (1971) Uber die Bestimmung von Funktionen durch ihre Integralwerte langs gewisser Maanigfaltigkeiten. Berichte Sachsische Akademie der Wissenschaften Leipzig, Math-Phys Kl 69:262
6. Munshi P, Rathore RKS, Vijay S (1994) A numerical investigation of an inverse theorem for computerized tomography. Eur J Non-destr Test 3:104
7. Razdan M, Kumar A, Munshi P (2006) Second level KT-1 signature of CT scanned medical images. Int J Tomogr Stat 4:20
8. Munshi P, Maisel M, Reiter H (1997) Experimental aspects of the approximate error formulae for tomographic reconstruction. Mater Eval 55(2):188
9. Munshi P (1988) Error estimates for the convolution back projection algorithm in computerized tomography. PhD Thesis, IIT Kanpur
10. Munshi P, Maisl M, Reter H (1995) Experimental study of tomographic contrast resolution. Nucl Instrum Methods Phys Res B95:402
11. Munshi P, Singh SP (1998) Hamming signature of three composite specimens. Res Nondestr Eval 10:109
12. Razdan M, Jauhari RK, Munshi P (2007) Analysis of pre and post-treatment CT images using KT-1 and fractal dimension. Trans Am Nucl Soc 346